University of Nevada, Reno

Use of a quartz crystal microbalance to investigate the mechanical stability of silica xerogel membranes for volatile iodine capture

A thesis submitted in partial fulfillment of the
requirements for the degree of Master of Science in
Materials Science and Engineering

by

Muhammad Ali

Dr. Krista Carlson/Thesis Advisor

December, 2022

THE GRADUATE SCHOOL

We recommend that the thesis
prepared under our supervision by

MUHAMMAD ALI

entitled

Use of a quartz crystal microbalance to investigate the mechanical stability of silica xerogel membranes for volatile iodine capture

be accepted in partial fulfillment of the
requirements for the degree of

MASTER OF SCIENCE

Krista Carlson, Ph.D.
Advisor

Dev Chidambaram, Ph.D.
Committee Member

Pradeep L. Menezes, Ph.D.
Graduate School Representative

Markus Kemmelmeier, Ph.D., Dean
Graduate School

December, 2022

ABSTRACT

There have been numerous studies on silica-based sorbents for the capture of radioiodine off-gassed during the processing of legacy waste or the reprocessing of nuclear waste. While studies investigate their iodine capture efficiency, only limited information about their mechanical applicability is found in the literature. This study investigates mechanical stability of silica-based adsorbents under the gas flow conditions to evaluate and quantify the effects of flow on the structural integrity of the tested materials. Silica-based xerogels, prepared through sol-gel processing using only tetraethoxysilane (TEOS), TEOS with oil as porogen, TEOS with bismuth nanoparticles, and TEOS with both. The technique subjected the adsorbents to a gas stream and used adhesive-coated quartz crystal, connected to a quartz crystal microbalance (QCM), to collect the particles lost by the adsorbents under flow. Collection of particles change the crystal's resonance, and the change is recorded on the QCM. The QCM data is analyzed to quantify the mass lost by the adsorbents. Adsorbents that did not contain bismuth failed under the flow as the QCM registered mass gains on the crystals, while the adsorbents with bismuth showed no failure. The results were supported by optical imaging that showed cracks on the failed surfaces. The technique used in this study showed encouraging results that validate the conceptualization of the technique as well as provide feedback for improvements to fine-tune technique for continued testing of new and existing materials.

TABLE OF CONTENTS

LIST OF TABLES

LIST OF FIGURES

1: INTRODUCTION

Presence of radioactive iodine in off-gas streams generated from aqueous reprocessing of spent nuclear fuel has been a major concern for the nuclear community. Radioactive iodine specie, ^{129}I, becomes part of the off-gas stream exhausted from the nuclear fuel reprocessing plants, or resulting from a nuclear accident. Because of its long half-life of over 16 million years and potential to penetrate in geological environments, iodine is required to be captured from the reprocessing plants. To capture iodine, a great attention has emerged toward exploring porous adsorbent materials, including functionalized activated carbon, zeolites, and silica [1-4].

Based on carbonaceous material, activated carbon is explored for iodine sorption because of its high surface area, allowance to tune pore structure, and economical industrial scale up [5]. While it offers encouraging efficacy toward the capture of gaseous iodine, water molecules in the stream have shown to decrease iodine capture as they take up most adsorption sites.

Silver-exchanged zeolites, such as mordenite and faujasite, are the benchmark materials for capturing iodine because of their low water solubility, large-scale commercial availability, and modest iodine capture efficiency [6-10]. While highly effective, these materials are difficult to transform into a dense waste form without the release of iodine [11]. Additionally, increasing concerns over silver toxicity necessitates further exploration toward alternate adsorbents, such as silica-based xerogels.

Silica-based xerogels can be synthesized using the sol-gel processing as it is a reliable and cost-effective technique to produce porous xerogels, using an alkoxide precursor such as tetraethoxysilane (TEOS) [12, 13]. The technique is followed by a suitable drying process such as supercritical drying, freeze drying or ambient pressure drying to remove the solvent content from the gels [14, 15]. Among these techniques, ambient pressure drying is the most economic technique and has not only gained extensive scientific attention but a huge industrial and commercial adoption as well [16]. These features, coupled with strong iodine affinity of considerably low toxic metal, bismuth, has shown development of a desirable product for iodine capture, as evident from our recent publication [17].

Naturally, the literature has widely investigated performance of these adsorbents toward static iodine capture of many such adsorbents but lacks the attention to examine their mechanical suitability in industrial application. Efforts have been made to estimate various mechanical properties of iodine sorbents such as hardness, Young's modulus, compressive strength, and strain-at-breaking using techniques such as nanoindentation, dynamic mechanical analysis and universal testing machine [18-24]. While these tests provide useful information for various aspects of material design and feasibility, they do not factor in complexities of dynamic gas flow through porous media and its mechanical effect on the microstructure and physical bonds between base material and metal, which can cause friable materials to disintegrate. Such a failure cannot be afforded when capturing iodine in reprocessing facilities [25-28]. It is, therefore, critical to evaluate

mechanical stability of any adsorbent intended to be used to capture iodine for their operational mechanical behavior [1, 2, 29-32].

This study designed, developed, and tested an experimental approach toward evaluating friability of several adsorbent materials by capturing and weighing any particles lost by the adsorbent under gas-flow conditions through a quartz crystal microbalance (QCM). QCM measures mass changes in a quartz crystal with sensitivity in the range of a few nanograms per unit area (ng/cm^2) [23, 33-35]. Quartz is a piezoelectric material with an ability to oscillate at a desired frequency given an appropriate potential difference, typically by using a gold electrode.[36, 37] Any mass loss from or mass gain on the electrode surface affects the resonating frequency of the crystal and is recorded through the QCM in real-time.

Evidence of QCM-based capture and weighing approach that closely follow the concept presented in this study can be found in studies targeted at atmospheric sensing of particulate matter (PM) and other harmful pollutants [38-41]. QCM-based sensors have been widely explored for measuring mass concentrations of atmospheric pollutants, including PM, as the QCM provides sensitive and rapid frequency shifts corresponding to mass gain on the crystal region [39]. To facilitate material lodging on the crystal region, researchers have achieved success coating the crystals using grease[41], photoresist film[38], and viscous media [42].

Our research group has published on porogen-assisted sol-gel processing of silica xerogels, which highlighted the monolithic nature of the xerogels that provides unique

advantages such as high specific surface area, tunability of pore structure as well as ability to be functionalized with metallic nanoparticles during the sol-gel processing [18]. These characteristics provide promising candidacy to silica xerogels to be explored as potential iodine adsorbents. Tuned-pore structure can lead to lower skeletal density which compromises the mechanical stability, and hence, for the purposes of this study, xerogels were prepared with and without porogen assistance. Furthermore, since iodine affinity is mostly achieved by functionalizing the adsorbent material with metal, this study also prepared and tested both xerogel variants – prepared with and without porogen assistance – with bismuth nanoparticles. Details of all 4 types of sample composition and their preparation is provided in Section 2.1, and Table 1.

1.1 Goal and objectives

The goal of this study was to develop a testing mechanism that can allow observation and quantification of mechanical stability of various silica xerogel compositions under gas flow condition. Fulfillment of this goal involved performing smaller objectives, including the synthesis of xerogels, development of the flow system with capture and weighing capabilities toward mass lost, setting up testing parameters, and subjecting the synthesized xerogels to the designed testing system for evaluation.

The first objective included synthesis of silica xerogels. Silica xerogels were selected to be tested for this study because of their promising features that make them viable candidates for iodine capture. This was also inspired from the fact that most xerogels can be weak as prepared and can be expected to present different mechanical stabilities

based on their composition. Hence, a pool of silica xerogels with varying compositions, as discussed in the method section, presented an opportunity to evaluate the efficacy of the designed system for mechanical testing.

The second objective was to develop the flow-based testing system. The system was targeted to capture particles that may disintegrate from the xerogel under the flow of gas, and subsequently weight them to quantify the failure. To this end, the QCM was used to provide sensitive weighing of the particles through its constantly resonating quartz crystal, which was coated with grease to facilitate the capture. The system followed a single-gas stream design that fed the temperature-controlled gas to the adsorbent at a certain volumetric flow and was extended to the quartz surface to allow for particle deposition before the stream was vented out.

Lastly, the third objective of the study was to subject the prepared xerogels to the designed system. To prepare the samples for testing, the prepared xerogels were needed to be housed in a leak-proof cartridge so that the gas can only travel by permeating through the xerogel. Furthermore, during the testing, the flowrate of the gas was needed to be kept in accordance with xerogels' capacity to saturate with. Higher flowrates can allow pressure build up in the adsorbent holder (discussed in Chapter 3), and can lead to test failure or equipment damage.

2: METHODS

2.1 Xerogel synthesis

Silica-based xerogels were made using sol-gel processing, a widely applied technique to convert a liquid silica source into a dried gel, through the use of adequate drying method.

The study targeted to produce crack-free silica gels and, as such, ambient drying technique was adopted that is known to allow favorable retention of pores. For this study, four types of samples were prepared: xerogel made with tetraethoxysilane (TEOS, 95% pure, Sigma Aldrich), with TEOS and soybean oil as porogen, with TEOS and bismuth nanoparticles, and with TEOS, soybean oil and bismuth nanoparticles. Nomenclature adopted to address these gels for this study is provided in Table 1.

Use of soybean oil as sacrificial porogen allows for creation of macropores, when the oil is removed, as evident in the literature [18]. Consequently, the gel prepared with macropores using porogen may offer high specific surface area, but can overall be compromised in its mechanical profile. Another key factor in preparing such adsorbents has been the proper functionalization, which in this study is performed with bismuth. It is likely that these particles can compensate for the loss of density and provide higher strength, and as such, the four compositions of samples adopted in this study allowed for comparative observations in terms of assessing the intrinsic mechanical stability as a result of available macropores, or bismuth particles, or both.

Detailed procedure adopted to synthesize the xerogels is provided in our previously published study [18]. Summarily, for TE, silica precursor (1.2 M TEOS) and hydrolysis (7.2

M water) solutions were prepared. For TEO, the precursor solution was added with 100 µL of soybean oil per 1 mL of combined sol-gel solution and the solution was vortexed for 1 min to homogenize oil with silica precursor. For TE-Bi, precursor solution was added with 5 w/v% bismuth nanoparticles, ultrasonicated for 15 min to ensure bismuth nanoparticles are properly mixed in silica precursor. For TEO-Bi, precursor solution was first added with 100 µL of soybean oil per 1 mL of combined sol-gel solution, vortexed for 1 m, added with 5 w/v% bismuth nanoparticles, ultrasonicated for 15 min to ensure both oil and nanoparticles are properly mixed in the silica precursor. To make the gels, both precursor and hydrolysis solutions were mixed and vortexed for 30 seconds, before the mixture was poured in a 10 mm circular mold made by removing the top of a flat-core rod syringe, shown in Figure 2-1. After allowing 10 min for gelation, the gels were kept in heptane to remove oil with solvent for 24 h in an oven at 30° C, after which another 24 h were allowed for the xerogels to dry in ambient pressure. Lastly, all the xerogels were kept at 150° C to allow for further drying and removal of any residual oil elements.

Table 1: Sample ID and composition.

Sample ID	Composition
TE	TEOS
TEO	TEOS + soybean oil
TE-Bi	TEOS + bismuth nanoparticles
TEO-Bi	TEOS + soybean oil + bismuth nanoparticles

Figure 2-1: Flat-core rod syringe used as a circular mold for gel preparation by removing the top.

2.2 Characterization of xerogels

The surface morphologies of all sample compositions were studied using SEM (JSM-7001F, JEOL and FEI Nova Nano, FEI, Inc.). SEM samples were prepared without any conducting surface coating.

The skeletal densities of all the sample compositions used in this study were obtained using He-pycnometer (Ultrapyc 5000; Anton Paar) with a micro-extension kit and a meso-cell with a nominal volume of 7.75 cm^3. Samples were dried at 150° C for 48 h to remove any trapped moisture before their skeletal densities were measured. Each test was allowed to run for 15 cycles with 5 saturations per cycle. Chamber pressure level was set to reach 19 psi during each saturation. The operational temperature of the pycnometer was set to 20° C throughout the experiments.

Backlit images of all the samples, after housing them in elastomer cartridge were taken before and after the experiments to visualize any physical effects caused by the gas flow on the samples during the experiment.

2.3 Experimental system and analysis

Figure 2-2 illustrates the experimental system used during this study to investigate mechanical behavior of silica-based adsorbents, hereon referred to as samples, under flow condition. The system includes a quartz crystal microbalance (eQCM 10M; Gamry Instruments), quartz crystals (Au-coated; Gamry Instruments) with a central frequency of 5 MHz, a crystal holder (Gamry Instruments) that can be connected to the QCM to

constantly read the resonance of the crystal, a custom-made sample holder made from glass as well as sample housing, and an incoming gas stream.

Once the crystal is fixed in the holder, one of the sides is connected to the QCM, while the other is coated with vacuum grease and is exposed to incoming gas stream. Vacuum grease is used to allow adhesion to any solid particles incoming gas stream. The crystal holder is connected to the incoming gas stream and the vent line using a 3D printed gas stream connector. To ensure maximum exposure of the crystal to gas stream, as well as better adhesion to the particles in the stream, the crystal holder is placed in a tilted fashion using a 3D printed crystal holder stand, as shown in Figure 2-3. The crystal holder is kept inside a column oven (CTO-20A; Shimadzu Scientific Instrument) to regulate the temperature during the experiment.

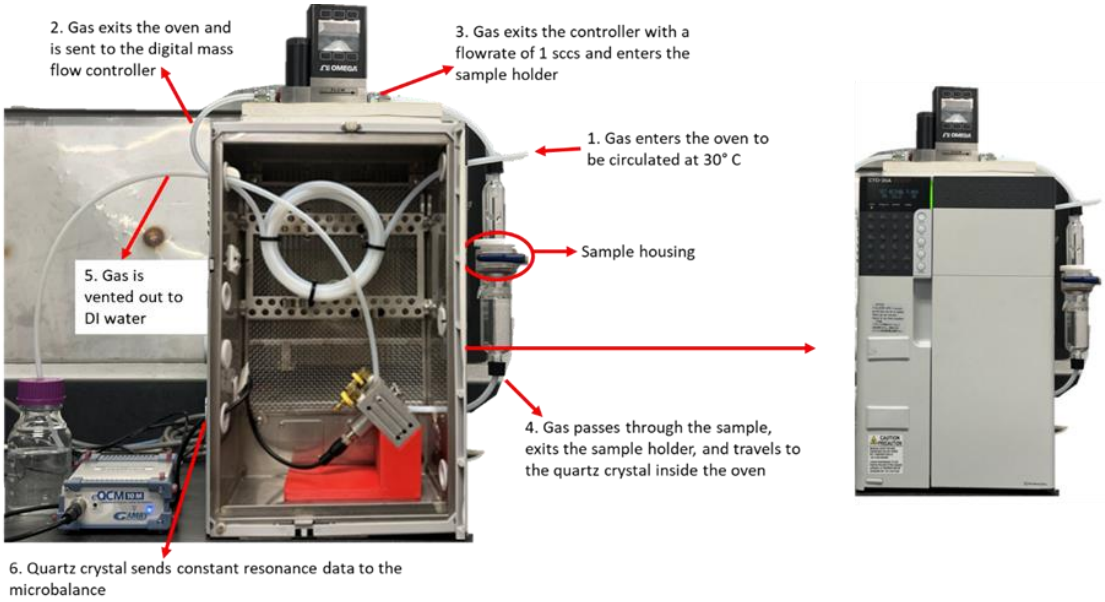

Figure 2-2: Experimental system used to investigate mechanical stability of the silica-based adsorbents.

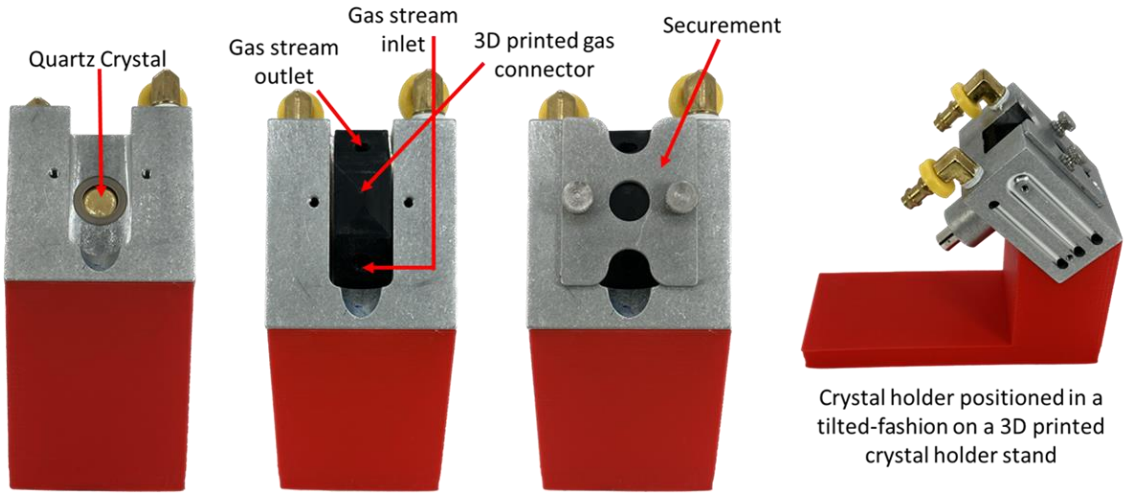

Figure 2-3: Tilted positioning of the crystal holder to provide crystal with maximum exposure to incoming gas stream.

The incoming gas stream from the tank is first transported in the column oven, circulated through the extended tubing to bring the carrier gas (Argon, Industrial Grade, Airgas and Linde) to the operational temperature (30° C), and then to the digital mass flow controller (FMA-2618A; Omega Engineering, Inc.) to regulate the flowrate. The stream from the controller is transported to the sample holder (positioned vertically with a downward flow to the gas), and then back inside the oven to the quartz crystal.

All sample compositions are tested with a flow of 1 sccs of industrial purity argon. Each test is run for a period of 12 h with the flow of gas. After 12 h, the gas is shut off, the sample is taken out, and the system is purged for 2 h with a higher flow to push any residual particles to the crystal that failed to reach the crystal due to lower flow during the experiment. The sample holder was washed between the tests to ensure any uncollected residue from previous experiment is removed. For TE and TEO, six samples were tested for each type, while for TE-Bi and TEO-Bi, only three samples for each sample composition were tested.

During the duration of the experiment, the resonance data is collected through the microbalance. Value of final change in frequency caused by the mass gain on the crystal at the end of the experiment is used in Sauerbrey's equation (Eq. 1) [43] to calculate the change in mass:

$$\Delta m = -C \,.A.\, \frac{\Delta f}{n} \qquad \text{Eq. 1}$$

where Δm is the change in mass, C is mass sensitivity constant of the quartz crystal, A is the resonating area of the crystal, n is the number of the harmonic, and Δf is the recorded change in frequency.

2.3.1 Sample and cartridge preparation

To place a sample inside the sample holder in a leak-proof fashion, the sample is first housed in a cartridge made from two-part silicone elastomer (base and curing agent; SYLGARD™ 184; Sigma-Aldrich) using 3D printed molds as shown in Figure 2-4. Average size of the silica-based samples prepared for this study is 10 mm in diameter and 3 mm in thickness. The molds were designed to these dimensions. To prepare the elastomer cartridge, the base and curing agent were mixed with a 10:1 ratio, and the mixture was brought to 25 mmHg absolute pressure to bring the trapped bubbles in the mixture to the top. The vacuum was then filled with ambient air to remove the bubbles. The process was repeated several times until all the bubbles were removed. The mixture was then poured into the molds and kept at 80° C, overnight, before removing the solidified cartridge parts from the molds. The molds and the two-part elastomer cartridge made from those molds are presented in Figure 2-3. Once the cartridge parts are removed from the molds, they are coated with glue, then a sample is inserted in one of the parts, and lastly, both parts are joined to make a sealed sample-containing cartridge that can then be inserted in the glass-based sample holder shown in Figure 2-5. The two-part cartridge design and the use of glue helped with providing a good seal to the sample, ensuring that the gas will only pass through the sample and not around it.

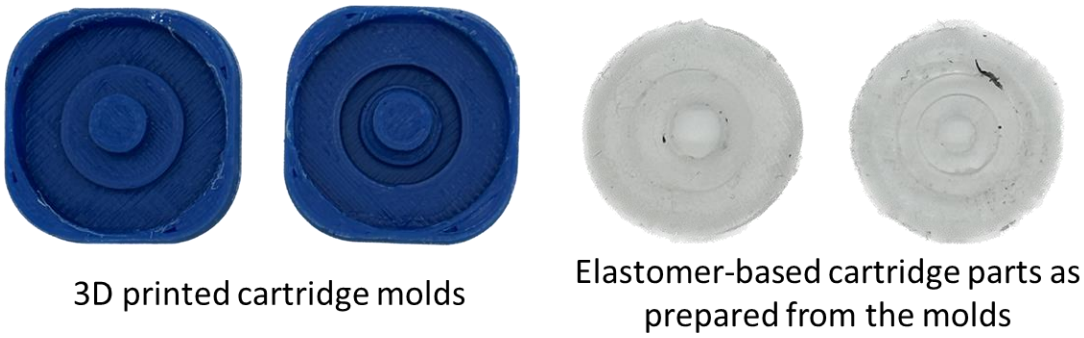

Figure 2-4: 3D-printed molds and elastomer-based cartridge parts for sample housing.

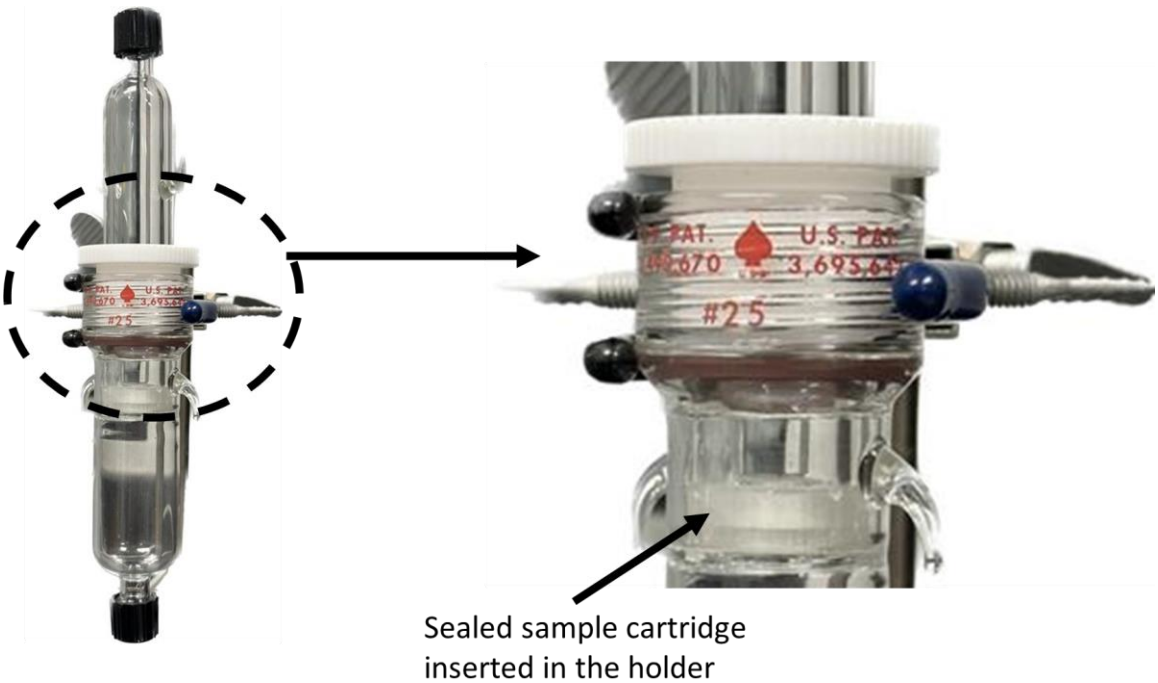

Figure 2-5: Sample cartridge holder, custom-made from glass, illustrating the sample fixation in the flow system.

3. RESULTS AND DISCUSSION

Figure 3-1 shows the prepared xerogels. From the SEM images (Figure 3-2), no macropores can be noticed in both TE and TE-Bi. Intrinsic surface roughness of silica prevents distinct observation of pore structure in TE. TEO and TEO-Bi show crater-like features due to the porogen with the diameter of the macroscale pores ranging between 5 and 20 µm (Figure 3-2b, and 3-2d).[18] Silica condensation during gelling reduces the miscibility with the oil and leads to forming distinct silica and oil regions, and as both regions grow, oil droplets are entrapped within the silica matrix. Their subsequent exchange with solvent and then drying leaves the microstructure with macropores, as evident in Figure 3-2b.

Both TE-Bi and TEO-Bi show clusters of bismuth nanoparticles throughout the surfaces, as observed from Figure 3-2c and 3-2d for TE-Bi and TEO-Bi, respectively. The nanoparticles preferred to cluster in the pores in presence of oil, with cluster sizes ranging from 5 µm to 20 µm. Yellow lines in Figure 3-2d point to the pores created through porogen assisted templating.

Measured skeletal densities of the samples are provided in Table 2. The results obtained from the flow experiments are presented in Figure 3-3, and their subsequent analysis with Sauerbrey's equation is presented in Table 2. Figure 3-3 shows that both TE and TEO sample compositions undergo mass loss, and Figure 3-4 shows cracks in TE and TEO as result of their failure during the flow. The general trend between both sample compositions is noticed as the graph show spikes, depicting the changes in resonance

frequency. TE and TEO have low skeletal density (Table 2), which is one of the important reasons for their weaker structural integrity, susceptible to breakage and material friability in gas flow condition, as the results show. Owing to the presence of macropores (Figure 3-2b), TEO has even weaker ability to maintain its structural integrity under flow. Therefore, TEO samples register more mass loss than TE samples during the QCM experiments. Although such macropores are not seen in TE, it still fails under flow, owing to its inherently weak internal structure as argued in numerous studies on silica xerogels.[28, 44-47]

As the first 12 h did not register any mass loss, TE-3 was allowed additional testing time. Allowing the experiment to continue showed a change in frequency after 16 h. The sample was removed soon after, and the system was purged. This suggests that TE and TEO may lose additional mass than recorded during the experiments at prolonged exposure to the flow conditions.

TE-Bi and TEO-Bi show no mass loss in any of the three samples tested per composition, and hence, only one representation per sample composition is presented in Figure 3-3.

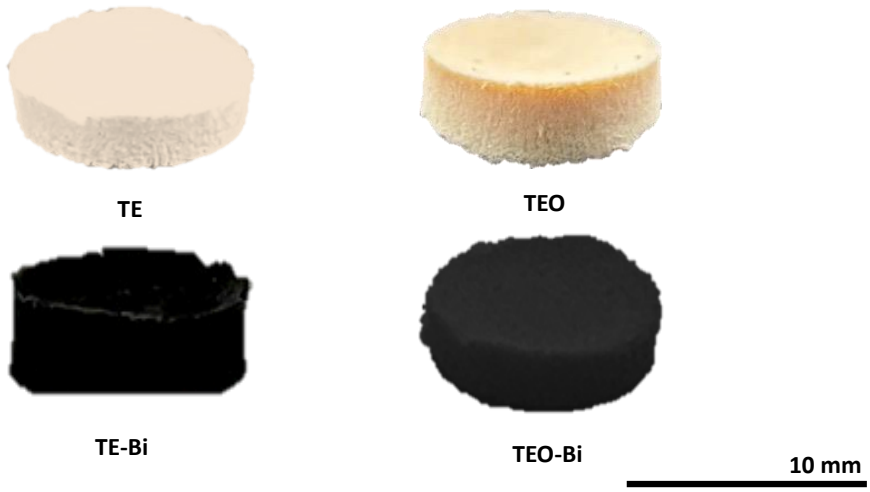

Figure 3-1: Xerogels prepared through sol-gel processing**.**

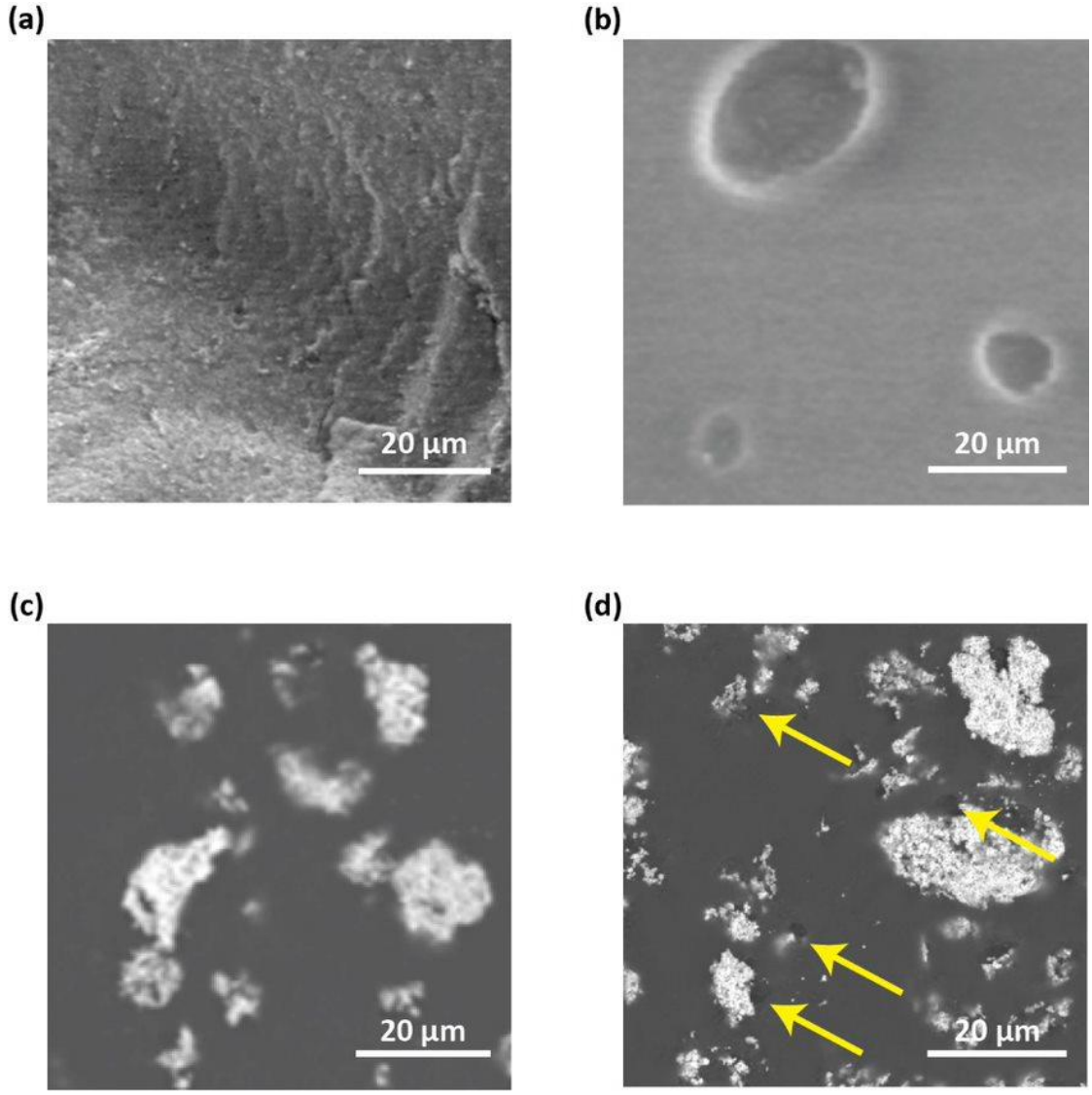

Figure 3-2: SEM images of TE (a) showing rough surface; TEO (b) showing macropores; TE-Bi (c) showing clusters of bismuth nanoparticles on a rough surface; and TEO-Bi (d) showing bismuth nanoparticles clusters and porogen assisted pores.

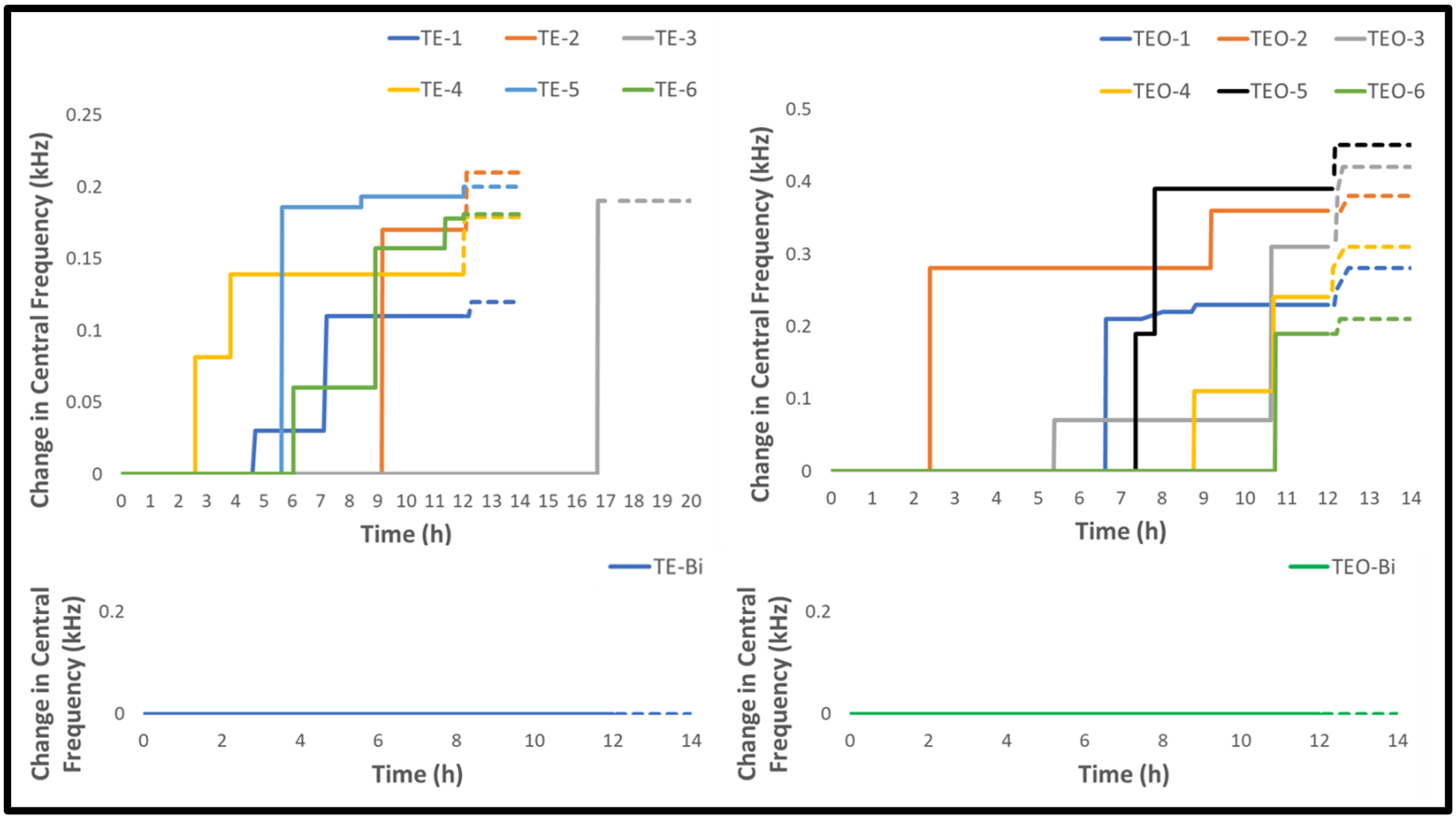

Figure 3-3: Visual representation of resonance data acquired on QCM. Changes in frequency are associated with mass loss from the corresponding sample because of the gas flow. TE and TEO show loss of mass, while TE and TE-Bi remain unaffected by the gas flow. Dotted lines represent the purging phase of the experiment.

Table 2: Corresponding values of mass loss from all the samples calculated using Saeurbrey's equation.

Sample ID	Change in Central Frequency (kHz)	Mass Loss (mg)	Initial Mass (g)	Percentage Mass Loss (%)	Avg. Mass Loss (mg)	Standard Deviation (mg)	Skeletal Density ($g.cm^{-3}$)
TE-1	0.12	0.011	0.132	0.008	0.02	0.003	1.99
TE-2	0.21	0.019	0.166	0.011			(0.165%)
TE-3	0.19	0.017	0.163	0.010			
TE-4	0.18	0.016	0.151	0.011			
TE-5	0.2	0.018	0.165	0.011			
TE-6	0.18	0.016	0.149	0.011			
TEO-1	0.28	0.025	0.168	0.015	0.03	0.008	1.90
TEO-2	0.38	0.034	0.172	0.020			(0.262%)
TEO-3	0.42	0.037	1.177	0.003			
TEO-4	0.31	0.027	0.17	0.016			
TEO-5	0.45	0.040	0.179	0.022			
TEO-6	0.21	0.019	0.159	0.012			
TE-Bi	0.00	0.000	0.22 (avg)	0.00	0.00	0.00	n/a
TEO-Bi	0.00	0.000	0.25 (avg)	0.00	0.00	0.00	n/a

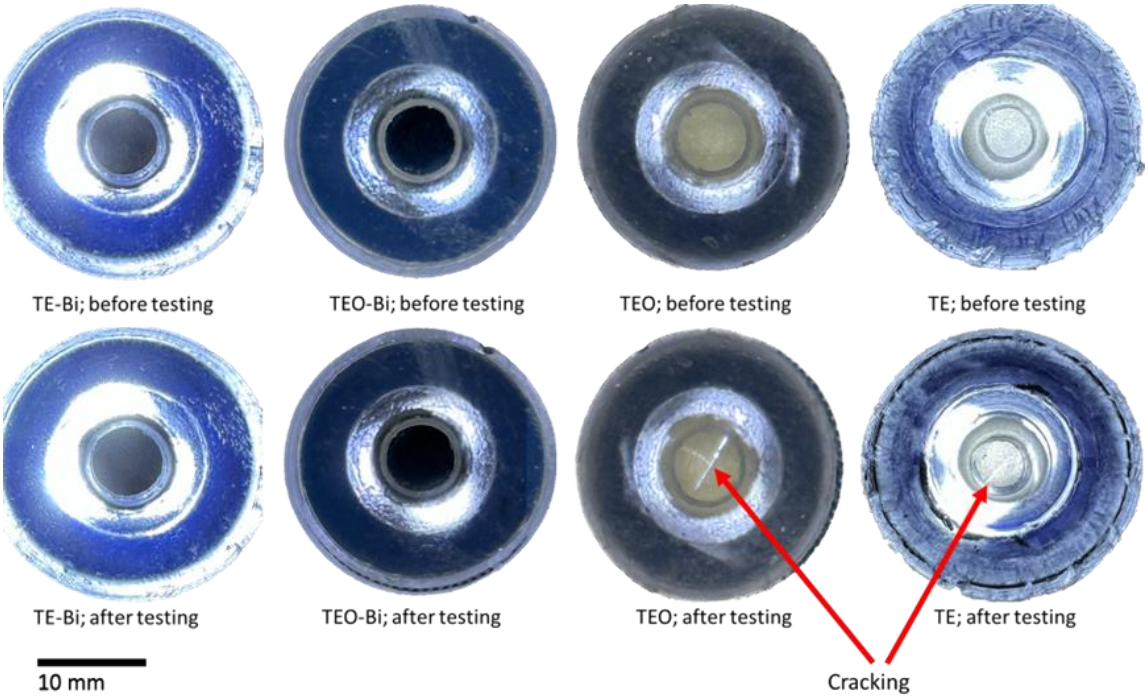

Figure 3-4: Backlit images for all sample compositions before and after the mechanical stability test.

TE-Bi and TEO-Bi benefitted from bismuth nanoparticles that provided better structural integrity as both bismuth containing xerogels remained unaffected throughout the tests. As evident in the backlit images provided in Figure 3-3, TE-Bi and TEO-Bi remain physically intact, while both TE and TEO fail and undergo cracking.

The flowrate was kept at a low rate of 1 sccs to ensure saturation with tested samples. While this low flowrate was observed to cause failure in TE and TEO, as they broke and allowed some of their particles to adhere to the crystal surface, it was observed that the flowrate failed to carry all the mass lost by those samples. Purging the system with higher flowrate after removing the sample allowed for residual particles to reach the crystal and register more mass change. Purging was performed in the absence of xerogel containing cartridge to enable higher flowrate that facilitated transporting residual particles to the crystal. This step proved to be crucial as it provided more reliability to the technique, ensuring that residual particles are transported to the crystal. This also highlights a critical limitation of the system, especially considering two examples, TEO-2 and TEO-6, where the former showed the first event of mass loss under 3 h, while the latter registered its first mass loss post 10 h. Since the sample composition was the same for both TEO-2 and TEO-6, this observation can be associated to variability in sample response under gas flow, but it can also be argued that one of the gels showed delayed mass loss because of the system's variability in terms of particle transport.

Using a vacuum grease to provide an adhesive layer is promising as a mass gain shown post 16 h during TE-3 experiment can be considered as an estimate of its long-lasting adhesion.

4. CONCLUSION

Mechanical stability of silica xerogels was tested using a QCM through a gas flow and capture system that subjected the xerogels to a gas stream and allowed for capture of any particles disintegrated from the xerogels. Capture of the particles by using the QCM system allowed for constant recording of change in resonance on the QCM, which was quantified to estimate the amount of mass loss from the xerogels.

The results showed TEO and TE to fail under the flow, and their failure was associated to their lower density profiles. TE-Bi and TEO-Bi showed no failure during the flow experiments. The results provide validity to the concept offered in the study as the trends observed from the results are supported by supplementary investigations, such as estimations of skeletal density, SEM, and backlit images, performed during the study.

The technique used in this study allowed the investigation of mechanical stability of xerogels, which is a critical parameter for adsorbent selection for industrial applications. Compared to conventional mechanical tests investigate bulk nature of the material, this technique provides observation into surface stability of the material, as surface regions mostly dictate material friability. The concept explored in this study has a potential to be applied in the cases where mechanical stability of adsorbent media under gas flow is an important factor. Industrial applications of the technique can benefit from designing a flow system that avoids necessitating purging to provide insight into effect of gas exposure duration on the materials.

References

1. Zhou, J., et al., *Highly efficient capture of iodine in spent fuel reprocessing off-gas by novelly porous copper-doped silica zeolites.* Separation and Purification Technology, 2022. **290**: p. 120895.
2. Shen, Z., et al., *Silver-functionalized silica aerogel for iodine capture: Adsorbent aging by NO2 in spent nuclear fuel reprocessing off-gas.* Microporous and Mesoporous Materials, 2022. **336**: p. 111898.
3. Al-Mamoori, A., et al., *Development of bismuth-mordenite adsorbents for iodine capture from off-gas streams.* Chemical Engineering Journal, 2020. **391**: p. 123583.
4. Reda, A.T., et al., *Bismuth-impregnated aluminum/copper oxide-pillared montmorillonite for efficient vapor iodine sorption.* Separation and Purification Technology, 2021. **270**: p. 118848.
5. Zhou, J., et al., *Study on adsorption performance of coal based activated carbon to radioactive iodine and stable iodine.* Annals of Nuclear Energy, 2014. **72**: p. 237-241.
6. Ayadi, T., et al., *Rational approach for an optimized formulation of silver-exchanged zeolites for iodine capture from first-principles calculations.* Molecular Systems Design & Engineering, 2022.
7. Jabraoui, H., et al., *Adsorption of volatile organic and iodine compounds over silver-exchanged mordenites: A comparative periodic DFT study for several silver loadings.* Applied Surface Science, 2019. **485**: p. 56-63.
8. Bruffey, S.H., R.T. Jubin, and J.A. Jordan, *Capture of elemental and organic iodine from dilute gas streams by silver-exchanged mordenite.* Procedia Chemistry, 2016. **21**: p. 293-299.
9. Scheele, R.D. and C.F. Wend, *Solidification and stabilization of silver mordenite used to control radioiodine emissions from Hanford's Waste Treatment Plant.* Annals of Nuclear Energy, 2015. **78**: p. 40-48.
10. Reiser, J.T., et al., *Review and experimental comparison of the durability of iodine waste forms in semi-dynamic leach testing.* Chemical Engineering Journal Advances, 2022. **11**: p. 100300.
11. Asmussen, R.M., et al., *Investigating the durability of iodine waste forms in dilute conditions.* Materials, 2019. **12**(5): p. 686.
12. Kato, M., K. Sakai-Kato, and T. Toyo'oka, *Silica sol-gel monolithic materials and their use in a variety of applications.* Journal of separation science, 2005. **28**(15): p. 1893-1908.
13. Ciriminna, R., et al., *The sol–gel route to advanced silica-based materials and recent applications.* Chemical reviews, 2013. **113**(8): p. 6592-6620.
14. Scherer, G.W., *Aging and drying of gels.* Journal of Non-Crystalline Solids, 1988. **100**(1-3): p. 77-92.
15. Scherer, G.W., *Recent progress in drying of gels.* Journal of non-crystalline solids, 1992. **147**: p. 363-374.
16. Aravind, P., et al., *Ambient pressure drying: a successful approach for the preparation of silica and silica based mixed oxide aerogels.* Journal of sol-gel science and technology, 2010. **54**(1): p. 105-117.
17. Baskaran, K., et al., *Effects of NO2 aging on bismuth nanoparticles and bismuth-loaded silica xerogels for iodine capture.* Journal of Hazardous Materials, 2022: p. 130644.

18. Baskaran, K., et al., *Membrane synthesis via in-situ pore formation in silica gels through dynamic miscibility with soybean oil.* Colloids and Surfaces A: Physicochemical and Engineering Aspects, 2022. **636**: p. 128183.
19. Baskaran, K., et al., *Evaluating the Physisorption and Chemisorption of Iodine on Bismuth-Functionalized Carbon Foams.* ACS Materials Letters, 2022. **4**: p. 1780-1786.
20. Rabbi, A., F. Dadashian, and M. Soleimani, *Evaluation of microporous acrylic-based activated carbon fibers as novel adsorbents for methylene blue removal.* Desalination and Water Treatment, 2020. **179**: p. 288-301.
21. Haefner, D., *Methods of gas phase capture of iodine from fuel reprocessing off-gas: a literature survey.* 2007.
22. Fukasawa, T., et al., *Application of silver impregnated iodine adsorbent to nuclear facilities.* Journal of Power and Energy Systems, 2008. **2**(1): p. 67-72.
23. Umadevi, K. and D. Mandal, *Performance of radio-iodine discharge control methods of nuclear reprocessing plants.* Journal of Environmental Radioactivity, 2021. **234**: p. 106623.
24. Sakuma, W., et al., *Mechanically strong, scalable, mesoporous xerogels of nanocellulose featuring light permeability, thermal insulation, and flame self-extinction.* ACS nano, 2021. **15**(1): p. 1436-1444.
25. Chong, S., et al., *Iodine Capture with Mechanically Robust Heat-Treated Ag–Al–Si–O Xerogel Sorbents.* ACS Omega, 2021. **6**(17): p. 11628-11638.
26. Flores-López, S.L., et al., *Effect of the porosity and microstructure on the mechanical properties of organic xerogels.* Journal of Materials Science, 2021. **56**(17): p. 10312-10325.
27. Gross, J., G. Reichenauer, and J. Fricke, *Mechanical properties of SiO2 aerogels.* Journal of Physics D: Applied Physics, 1988. **21**(9): p. 1447.
28. Maleki, H., L. Durães, and A. Portugal, *An overview on silica aerogels synthesis and different mechanical reinforcing strategies.* Journal of Non-Crystalline Solids, 2014. **385**: p. 55-74.
29. Parmenter, K.E. and F. Milstein, *Mechanical properties of silica aerogels.* Journal of non-crystalline solids, 1998. **223**(3): p. 179-189.
30. Arvidson, J.M. and L.L. Scull, *Compressive Properties of Silica Aerogel at 295, 76, and 20 K*, in *Advances in Cryogenic Engineering Materials*, R.P. Reed and A.F. Clark, Editors. 1986, Springer US: Boston, MA. p. 243-250.
31. Murillo, J.S.R., et al., *Structure and mechanical properties of silica aerogels and xerogels modeled by molecular dynamics simulation.* Journal of non-crystalline solids, 2010. **356**(25-27): p. 1325-1331.
32. Matyas, J., et al. *Functionalised silica aerogels: Advanced materials to capture and immobilise radioactive iodine*. in *Ceramic Engineering and Science Proceedings*. 2011. American Ceramic Society, Inc., 735 Ceramic Place Westerville OH 43081 ….
33. Lee, T., *Assessment of safety culture at a nuclear reprocessing plant.* Work & Stress, 1998. **12**(3): p. 217-237.
34. Jubin, R., D. Strachan, and N. Soelberg, *Iodine pathways and off-gas stream characteristics for aqueous reprocessing plants–A literature survey and assessment.* 2013.
35. Wershofen, H. and D. Aumann, *Iodine-129 in the environment of a nuclear fuel reprocessing plant: VII. Concentrations and chemical forms of 129I and 127I in the atmosphere.* Journal of environmental radioactivity, 1989. **10**(2): p. 141-156.

36. O'sullivan, C. and G. Guilbault, *Commercial quartz crystal microbalances–theory and applications.* Biosensors and bioelectronics, 1999. **14**(8-9): p. 663-670.
37. Mecea, V.M., *From quartz crystal microbalance to fundamental principles of mass measurements.* Analytical Letters, 2005. **38**(5): p. 753-767.
38. Zhao, J., et al., *Airborne particulate matter classification and concentration detection based on 3D printed virtual impactor and quartz crystal microbalance sensor.* Sensors and Actuators A: Physical, 2016. **238**: p. 379-388.
39. Ngo, N.D., et al., *Measurement of PM 2.5 mass concentration using an electrostatic particle concentrator-based quartz crystal microbalance.* IEEE Access, 2019. **7**: p. 170640-170647.
40. Amaral, S.S., et al., *An overview of particulate matter measurement instruments.* Atmosphere, 2015. **6**(9): p. 1327-1345.
41. Zampetti, E., et al., *Exploitation of an integrated microheater on QCM sensor in particulate matter measurements.* Sensors and Actuators A: Physical, 2017. **264**: p. 205-211.
42. Sem, G.J., K. Tsurubayashi, and K. HOMMA, *Performance of the piezoelectric microbalance respirable aerosol sensor.* American Industrial Hygiene Association Journal, 1977. **38**(11): p. 580-588.
43. Huang, X., et al., *A practical model of quartz crystal microbalance in actual applications.* Sensors, 2017. **17**(8): p. 1785.
44. Lee, K.-Y., et al., *Composites of silica aerogels with organics: A review of synthesis and mechanical properties.* Journal of the Korean Ceramic Society, 2020. **57**(1): p. 1-23.
45. Baskaran, K., et al., *Sol-gel derived silica: A review of polymer-tailored properties for energy and environmental applications.* Microporous and Mesoporous Materials, 2022: p. 111874.
46. Maleki, H., L. Durães, and A. Portugal, *A new trend for development of mechanically robust hybrid silica aerogels.* Materials Letters, 2016. **179**: p. 206-209.
47. Mackenzie, J.D., Q. Huang, and T. Iwamoto, *Mechanical properties of ormosils.* Journal of Sol-Gel Science and Technology, 1996. **7**(3): p. 151-161.